Geophysical Research Letters

RESEARCH LETTER
10.1029/2021GL096018

Key Points:

- An ocean circulation inverse model is used to quantify abiotic air-sea CO_2 fluxes from 1780 to 2020
- Increasing atmospheric pCO_2 drives the multidecadal trend in ocean CO_2 uptake, which averages 2.7 PgC yr^{-1} from 2010 to 2020
- Ocean circulation and biology are implicated as the main drivers of decadal variability of the ocean CO_2 sink

Supporting Information:

Supporting Information may be found in the online version of this article.

Correspondence to:

T. DeVries,
tdevries@geog.ucsb.edu

Citation:

DeVries, T. (2022). Atmospheric CO_2 and sea surface temperature variability cannot explain recent decadal variability of the ocean CO_2 sink. *Geophysical Research Letters*, *49*, e2021GL096018. https://doi.org/10.1029/2021GL096018

Received 2 SEP 2021
Accepted 1 MAR 2022

Atmospheric CO_2 and Sea Surface Temperature Variability Cannot Explain Recent Decadal Variability of the Ocean CO_2 Sink

Tim DeVries[1,2]

[1]Department of Geography, University of California, Santa Barbara, Santa Barbara, CA, USA, [2]Earth Research Institute, University of California, Santa Barbara, Santa Barbara, CA, USA

Abstract The ocean is one of the most important sinks for anthropogenic CO_2 emissions. Here, I use an ocean circulation inverse model (OCIM), ocean biogeochemical models, and pCO_2 interpolation products to examine trends and variability in the oceanic CO_2 sink. The OCIM quantifies the impacts of rising atmospheric CO_2, changing sea surface temperatures, and gas transfer velocities on the oceanic CO_2 sink. Together, these effects account for an oceanic CO_2 uptake of 2.2 ± 0.1 PgC yr^{-1} from 1994 to 2007, and a net increase in the oceanic carbon inventory of 185 PgC from 1780 to 2020. However, these effects cannot account for the majority of the decadal variability shown in data-based reconstructions of the ocean CO_2 sink over the past 30 years. This implies that decadal variability of the ocean CO_2 sink is predominantly driven by changes in ocean circulation or biology that act to redistribute both natural and anthropogenic carbon in the ocean.

Plain Language Summary The ocean currently absorbs about 25% of industrial CO_2 emissions, but there are numerous factors that can cause variation in the rate of ocean CO_2 uptake over time. This study uses a combination of observation-based models to investigate the causes of variability in the rate of ocean CO_2 uptake. The results show that the long-term trend of ocean CO_2 uptake is driven mainly by increasing atmospheric CO_2 concentrations, but the variability from that trend is due mostly to changes in the distribution of CO_2 in the ocean that are caused by changes in ocean circulation and biology.

1. Introduction

The ocean currently absorbs roughly 25% of anthropogenic CO_2 emissions (Friedlingstein et al., 2019) and is the largest net carbon sink for anthropogenic CO_2 over the industrial era (Khatiwala et al., 2009). Recent work has shown that the oceanic CO_2 sink is variable on interannual to decadal time scales with temporal variability of ~10%–20% of the global mean (Landschützer et al., 2016; Rödenbeck et al., 2015). The most significant feature of the ocean CO_2 sink over the past 30 years was a stagnation or weakening of the ocean CO_2 sink in the 1990s, followed by an acceleration of the global ocean carbon sink in the following decades (DeVries et al., 2017, 2019; Landschützer et al., 2015). The mechanisms driving these global-scale changes in the strength of the ocean CO_2 sink remain uncertain. A recent study proposed that these changes were driven by variability in the growth rate of atmospheric CO_2 along with changes in the sea surface temperature (SST) caused by the eruption of Mt. Pinatubo in 1991 (McKinley et al., 2020), while other studies have suggested that these changes were driven by a redistribution of carbon in the ocean due to variability associated with climate modes (Landschützer et al., 2015, 2016) and changes in ocean circulation (DeVries et al., 2017; Gruber, Landschützer, & Lovenduski, 2019; Gruber, Clement, et al., 2019).

These different hypotheses regarding the drivers of variability in the ocean CO_2 sink can be understood in terms of the mechanisms affecting the air-sea CO_2 flux (Figure 1). This flux is driven by the pressure gradient between CO_2 in seawater and air and further modulated by the solubility of CO_2 in seawater (α) and the air-sea gas transfer velocity (K_w) via the bulk formula,

$$F_{air-sea} = \alpha K_w \left(pCO_{2,sw} - pCO_{2,air}\right). \quad (1)$$

The mechanisms proposed by McKinley et al. (2020) drive variability in $F_{air-sea}$ through variations in atmospheric pCO_2 ($pCO_{2,air}$) and SST (through its effect on α, the CO_2 solubility in seawater), while mechanisms that invoke

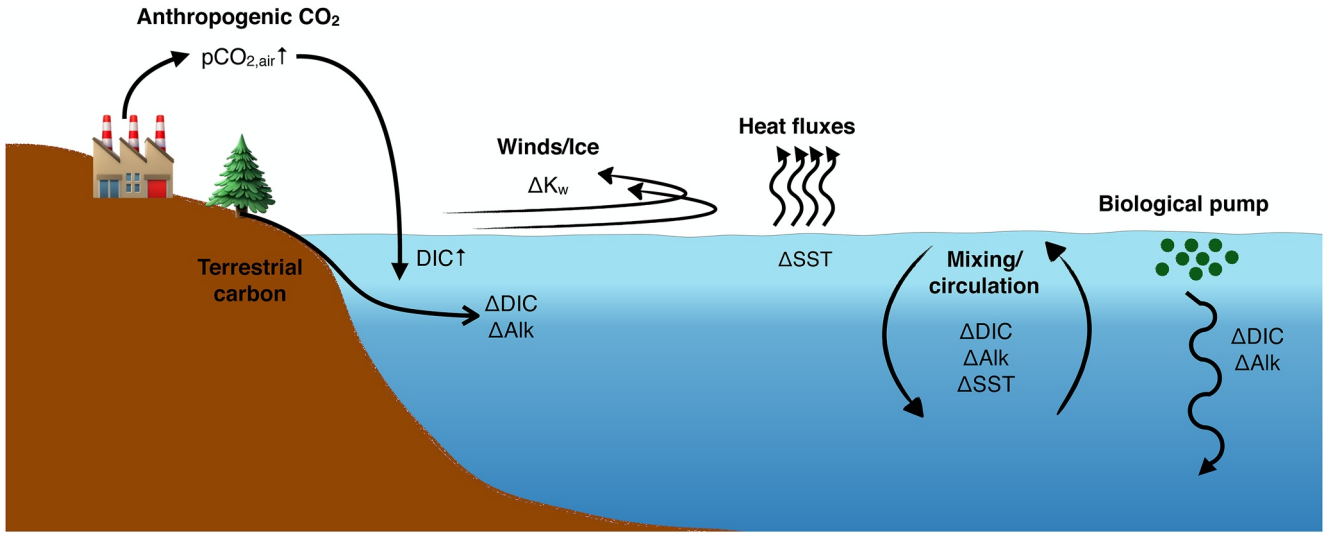

Figure 1. Schematic diagram illustrating the mechanisms affecting air-sea CO_2 fluxes. Anthropogenic CO_2 emissions drive an increase in atmospheric pCO_2 ($pCO_{2,air}$) and a long-term influx and accumulation of anthropogenic carbon in the ocean (Mikaloff Fletcher et al., 2006; Sabine et al., 2004; Sarmiento et al., 1992). The air-sea exchange of CO_2 is further influenced by changes in the CO_2 solubility (α) due to changes in sea-surface temperatures driven by air-sea heat fluxes or ocean mixing; by changes in winds and sea ice that influence the gas transfer velocity (K_w); by the internal redistribution of DIC and alkalinity by ocean circulation, mixing, and the biological pump, which affect seawater pCO_2 ($pCO_{2,sw}$); and by the influx of terrestrial carbon and alkalinity to the ocean. Terrestrial carbon includes inputs from rivers, submarine groundwaters, and coastal vegetation (Kwon et al., 2021).

ocean circulation changes propose that the variability in $F_{air-sea}$ is driven by internal redistributions of dissolved inorganic carbon (DIC) and alkalinity in the ocean, which influence the seawater pCO_2 ($pCO_{2,sw}$).

Here, I test the hypothesis that the recent variability of the ocean CO_2 sink can be explained by the observed variability of ocean surface temperatures and atmospheric pCO_2 without invoking any changes in ocean circulation or biology. To test this hypothesis, I use a new version of the steady-state ocean circulation inverse model (OCIM; DeVries, 2014) to quantify air-sea CO_2 fluxes that arise from observed changes in atmospheric pCO_2 and SST as well as surface winds and sea ice that drive changes in the gas transfer velocity (Figure 1; Section 2). The global $F_{air-sea}$ diagnosed from this model is compared to that derived from a suite of global ocean biogeochemical models (GOBMs) and pCO_2-based flux products (Section 3). I compare the magnitude, trends, and variability of CO_2 fluxes from each of these methods with a focus on the decadal variability of air-sea CO_2 fluxes (Section 3). This comparison reveals that variations in atmospheric pCO_2 and SST alone do not account for the majority of the decadal variability of the ocean CO_2 sink reconstructed by biogeochemical models and pCO_2-based products (Section 3). This implicates changes in ocean circulation and/or biology as the main driving forces of decadal variability of the global ocean CO_2 sink. I close by discussing remaining uncertainties and providing suggestions for future work (Section 4).

2. Methods

2.1. Ocean Circulation Inverse Model (OCIM)

The OCIM is a three-dimensional dynamical ocean model that assimilates ocean tracer data to estimate the climatological mean state of the ocean circulation. Previous versions of the OCIM have been described in DeVries and Primeau (2011) (OCIM0), DeVries (2014) (OCIM1), and DeVries and Holzer (2019) (OCIM2), and details regarding the model formulation can be found in those publications. The version used here is called OCIM2-48L and was described in a recent study of the ventilation of the deep Pacific (Holzer et al., 2021). The tracers assimilated by OCIM2-48L include temperature, salinity, radiocarbon, CFC-11, CFC-12, and δ^3He, and additional constraints on the model solution include the mean dynamical sea-surface topography, and air-sea fluxes of heat and freshwater. An adjoint approach (Schlitzer, 1993, 2007) is used to find the optimal model parameters that minimize the difference between the model and observations (DeVries & Primeau, 2011). The OCIM2-48L is similar to the OCIM1 used in a previous study to estimate global ocean anthropogenic CO_2 uptake (DeVries, 2014)

with some updates and improvements. The major improvements are a doubling of the vertical resolution from 24 levels to 48 levels, an improved parameterization for the vertical diffusivity using a tidal energy dissipation model (de Lavergne et al., 2019, 2020), and inclusion of isopycnal diffusivities in the model's adjustable parameters. A full list of differences between OCIM2-48L and OCIM1 and a comparison between modeled and observed tracers can be found in the Supporting Information (Figure S1 in Supporting Information S1). Like all the previous OCIM versions, OCIM2-48L neglects temporal (e.g., seasonal or interannual) variability in ocean circulation and thus represents a climatological steady state.

2.2. CO_2 Simulations Using OCIM2-48L

The optimized advective and diffusive transport from the OCIM2-48L is stored offline as a transport matrix (Khatiwala et al., 2005; Kwon & Primeau, 2006) and is used to simulate DIC in the ocean using an abiotic model. The governing equation for this model is

$$\frac{\partial \mathrm{DIC}}{\partial t} = \mathbf{A}\mathrm{DIC} - \frac{F_{air-sea}}{\delta z_1}, \tag{2}$$

where **A** is the transport matrix operator, δz_1 is the depth of the top model layer (10 m), and $F_{air-sea}$ is the time-varying air-sea CO_2 gas exchange flux given by Equation 1. Atmospheric CO_2 was derived from a compilation of NOAA field stations for the years 1958–2020 and from ice core data (Macfarling Meure et al., 2006) prior to that (see Figure S2 in Supporting Information S1). Seawater pCO_2 was calculated from the modeled DIC field and the observed sea-surface alkalinity from the Global Ocean Data Analysis Project v2 objectively mapped total alkalinity field (Lauvset et al., 2016). CO_2 solubility and equilibrium constants were computed using climatological salinity from the World Ocean Atlas (Zweng et al., 2013) and time-varying monthly SST fields from various reanalysis products (see Figure S3 in Supporting Information S1). The gas transfer velocity K_w is parameterized as a quadratic function of wind speed and proportional to the fraction of ice-free ocean in each grid cell (Wanninkhof et al., 2013). Wind speeds and sea ice fraction were taken from the NCEP reanalysis (Behringer & Xue, 2004). The Supporting Information provides further information on the input products.

The model is spun up to a cyclostationary steady state under monthly forcing for year 1780, and then a transient simulation is run from 1780 to 2020 at monthly resolution. Although the surface forcing is monthly and includes seasonal variability, the ocean transport model is steady state, and seasonal variability in circulation and mixing are not simulated. Six different simulations are performed. In the first three simulations (A–C, Table S1 in Supporting Information S1), the atmospheric pCO_2 is varied over time but the SST is held constant. In the second three simulations (D–F, Table S1 in Supporting Information S1), the atmospheric pCO_2 and SST are both varied according to the observations (Figure S3 in Supporting Information S1). All simulations use a time-variable gas transfer velocity. Simulations (D–F) are used to test the hypothesis that recent decadal variability in ocean CO_2 uptake is driven by the variability in the atmospheric CO_2 growth rate and sea surface temperatures.

Several caveats should be noted regarding the model results. First, the OCIM2-48L does not include the biological cycling of CO_2 and therefore, the natural DIC distribution in the OCIM2-48L is different from that in the real ocean. Therefore, the influence of changes in atmospheric pCO_2 and SST on the air-sea CO_2 flux will be different in the abiotic ocean simulated by the OCIM than in the real ocean due to differences in the seawater DIC distribution and the resulting buffer capacity (Watson & Orr, 2003). However, simulations with the OCIM2-48L that include steady-state biological carbon fluxes from a data-constrained biological pump model (DeVries & Weber, 2017) have global air-sea CO_2 fluxes that are nearly identical to those from the abiotic model (Figure S4 in Supporting Information S1), demonstrating that the influence of an unchanging biological carbon cycle on these results is minimal. Finally, CO_2 solubility can also be affected by changes in sea surface salinity, which is not considered in the OCIM2-48L since the variability of salinity is much smaller than that of temperature.

2.3. GOBMs

Global air-sea CO_2 fluxes from the OCIM2-48L simulations are compared to those from hindcast GOBMs for the period 1959–2020. Global air-sea CO_2 fluxes for eight different GOBMs were obtained from the 2021 Global Carbon Budget (Aumont et al., 2015; Berthet et al., 2019; Doney et al., 2009; Hauck et al., 2020; Lacroix et al., 2021; Liao et al., 2020; Schwinger et al., 2016; Wright et al., 2021). Like the OCIM2-48L simulations,

Table 1
Mechanisms of Variability in Air-Sea CO_2 Fluxes Captured by Each of the Methods Discussed Here

Model	pCO_2^{air}	α and K_w	Circulation and biology	Terrestrial inputs
OCIM2-48L	✓	✓		
GOBMs	✓	✓	✓	
pCO_2 reconstructions	✓	✓	✓	✓

the GOBMs include time-varying atmospheric pCO_2. They also include time-varying surface heat fluxes and gas transfer velocity prescribed from reanalysis products, which produce variable SST and CO_2 solubilities in the model. Unlike the OCIM2-48L, the GOBMs also capture variability in air-sea CO_2 fluxes driven by redistributions of DIC and alkalinity due to changing ocean circulation and biological fluxes (Figure 1; Table 1).

2.4. Data-Based pCO_2 Reconstructions

Global air-sea CO_2 fluxes from four different data-based pCO_2 reconstructions are also used for comparison. These products are all based on the Surface Ocean CO_2 Atlas (SOCAT) data set of seawater pCO_2 observations (Bakker et al., 2016), but use different methods to interpolate gaps in that data set to produce global monthly maps of $pCO_{2,sw}$ from roughly the mid-1980s to 2020. Each group uses these interpolated $pCO_{2,sw}$ maps, along with reanalysis SST and gas transfer velocities, to calculate the air-sea CO_2 flux according to Equation 1. The products used here are four of the products used in the 2021 Global Carbon Budget (Chau et al., 2021; Gregor et al., 2019; Landschützer et al., 2016; Rödenbeck et al., 2014). Air-sea CO_2 fluxes calculated from these data-based pCO_2 reconstructions capture all sources of variability in air-sea CO_2 fluxes (Figure 1; Table 1). One distinction between the pCO_2-based flux products and the GOBMs is that the pCO_2 reconstructions implicitly include the effects of terrestrial carbon inputs on the seawater pCO_2, while those inputs are not included in the GOBMs. For the pCO_2 interpolation products, we only use data for 1990 onward, because uncertainties prior to 1990 are large due to a lack of pCO_2 observations.

3. Results and Discussion

The globally integrated air-sea CO_2 flux from the OCIM2-48L simulations D–F is shown in Figure 2a. The flux is always negative due to rising atmospheric pCO_2 and the invasion of anthropogenic CO_2 into the ocean. Since 1960, there is a nearly linear increase in global ocean CO_2 uptake, reaching a value of 2.9 PgC yr^{-1} in 2020. The mean uptake over the time period 1994–2007 is 2.2 PgC yr^{-1}, which is somewhat smaller than the anthropogenic CO_2 accumulation of 2.6 ± 0.3 PgC yr^{-1} derived from ocean interior DIC observations for the same period (Gruber, Clement, et al., 2019). Simulations A–C, which do not include variable SST, yield an average ocean uptake of 2.4 PgC yr^{-1} for 1994–2007, which is close to the ocean CO_2 uptake of 2.5 PgC yr^{-1} from the OCIM1 (DeVries, 2014; Figure S5 in Supporting Information S1; see Section 1.5 in Supporting inforamtion S1 for a detailed comparison of the OCIM1 and the OCIM2-48L results). The ocean DIC inventory increased by 183 ± 6 PgC from 1780 to 2020 in the OCIM2-48L simulations D–F (Figure 2b). The total accumulation of DIC in simulations A–C (i.e., neglecting the change in DIC inventory due to changes in SST) is 192 ± 0.2 PgC as of 2020. The change in ocean carbon inventory over time in the OCIM2-48L agrees with estimates of anthropogenic CO_2 accumulation based on ocean interior DIC observations (Gruber, Clement, et al., 2019; Sabine et al., 2004), the OCIM1 (DeVries, 2014) and a compilation of data- and model-based estimates of oceanic anthropogenic CO_2 uptake (Khatiwala et al., 2013; Figure 2b).

The spatial distribution of DIC accumulation since 1960, when direct atmospheric CO_2 measurements become available, reflects a combination of air-sea CO_2 fluxes and ocean circulation patterns (Figure 3). The North Atlantic has the highest column inventory of accumulated DIC due to the uptake of anthropogenic CO_2 associated with upwelling in the subpolar gyre (Sarmiento et al., 1992) and the formation of deep waters in the Labrador Sea (Rhein et al., 2002) and Greenland-Iceland-Norwegian Seas (Chafik et al., 2020; Fröb et al., 2016). In these regions, anthropogenic CO_2 is fed into deep water masses, which flow southward predominantly along the deep western boundary current, leading to high column inventories of accumulated DIC in the western North Atlantic (Figure 3a). Substantial DIC accumulation is also found in the subpolar Southern Ocean and the northwest Pacific (Figure 3a), where anthropogenic CO_2 is subducted into the interior ocean in regions of intermediate and mode water formation (Waters et al., 2011; Murata et al., 2009). The weakest DIC accumulation is found in the poorly ventilated regions of the Eastern Tropical Pacific (ETP), coincident with the presence of oxygen minimum zones in these regions. The vast majority of the DIC that has accumulated in the ocean since 1960 is due to rising atmospheric CO_2 concentrations (Figure 3b) (Figure S6 in Supporting Information S1 compares these results to

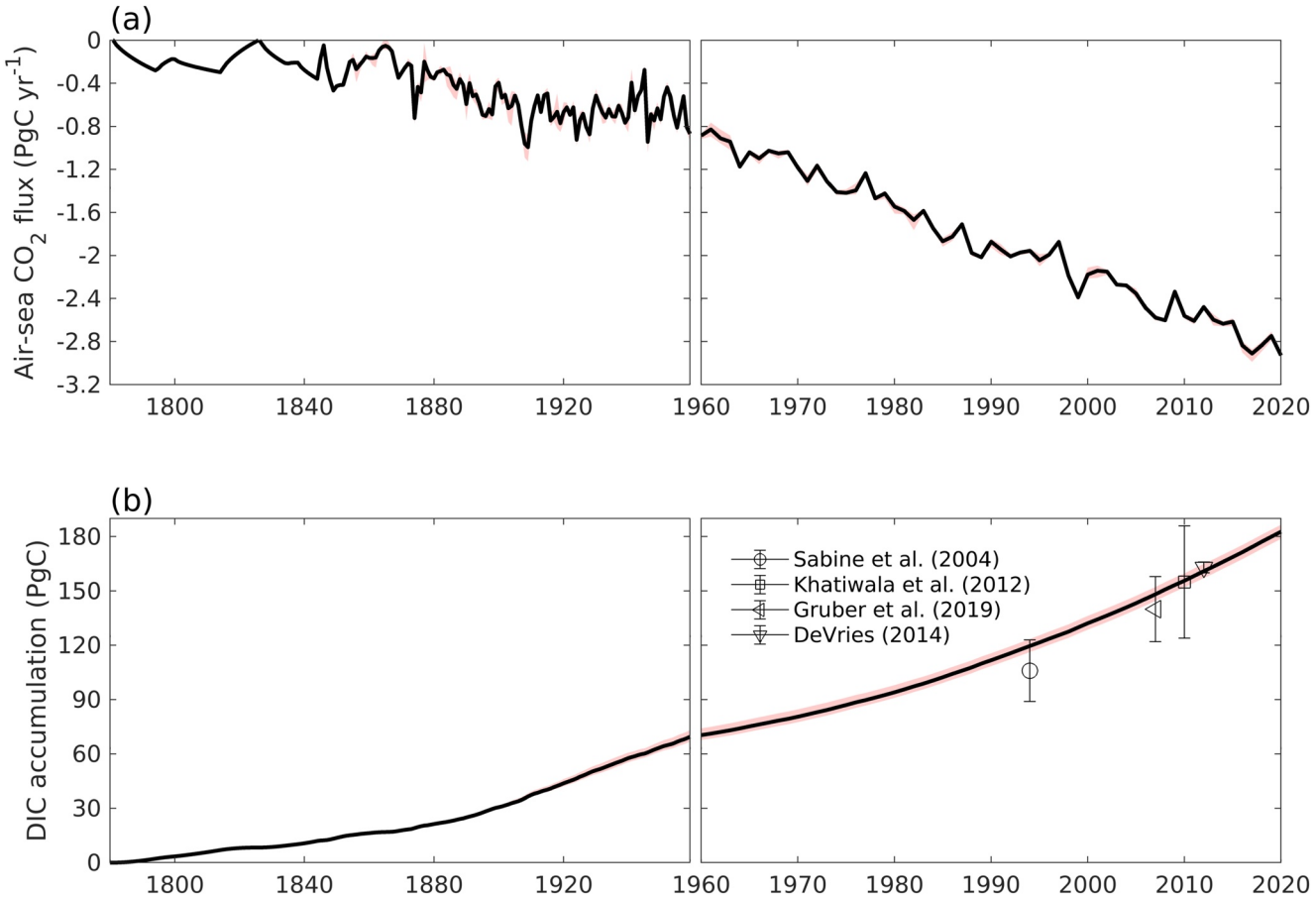

Figure 2. (a) Globally integrated air-sea CO_2 fluxes from OCIM2-48L simulations that capture variability in atmospheric pCO_2, sea surface temperature, and gas transfer velocity (simulations D–F, Table S1 in Supporting Information S1) for the period 1780–2020. Negative fluxes indicate the uptake of CO_2 by the ocean. (b) Total dissolved inorganic carbon accumulated in the ocean since 1780 from the same simulations compared to some other recent estimates of the oceanic inventory of anthropogenic CO_2. The bold line is the mean of all three simulations, and the red shading covers the full range of simulations.

prior estimates of the anthropogenic CO_2 inventory from the OCIM1 (DeVries, 2014) and an observation-based regression model (Gruber, Clement, et al., 2019).) Variations in SST affect the CO_2 solubility and alter the oceanic DIC inventory with the predominant effect being a decrease in the DIC inventory driven by warming of surface waters, which reduces CO_2 solubility (Figure 3c). The largest warming-driven decreases in DIC inventory occur in the subpolar Southern Ocean (Figure 3c). Since 1960, the net effect of ocean warming has been a reduction of the ocean DIC inventory by 8 ± 2 PgC (5 ± 1 PgC since 1990).

The air-sea CO_2 fluxes from the OCIM2-48L can be compared to those from GOBMs and pCO_2 interpolation products (Figure 4). All three methods show a trend toward increased ocean CO_2 uptake over time (Figure 4a). However, fitting a linear regression to the global air-sea CO_2 flux over the period 1990–2020 demonstrates that the three methods have different trends. The pCO_2 interpolation products show the strongest trend at roughly -0.05 PgC yr^{-2}, followed by the OCIM2-48L at -0.034 PgC yr^{-2}, with the GOBMs having the weakest trend at -0.026 PgC yr^{-2} (Table 2). Furthermore, the mean air-sea CO_2 flux over the period 1990–2020 is different across the three different methods ranging from roughly -1.8 PgC yr^{-1} in the pCO_2 interpolation products to -2.4 PgC yr^{-1} in the OCIM2-48L (Table 2). The lower mean air-sea CO_2 flux found by the interpolation products is often attributed to the outgassing of terrestrially derived (i.e., riverine) CO_2 that is captured by the pCO_2 products, but not by the GOBMs or the OCIM2-48L (Friedlingstein et al., 2019; Resplandy et al., 2018; Table 1). The stronger trend in the pCO_2 interpolation products relative to the GOBMs has been noted in the 2021 Global Carbon Budget (Friedlingstein et al., 2021), but the reasons for this discrepancy are unknown. The analysis that follows focuses on the variability of the air-sea CO_2 flux about the linear trend for each method.

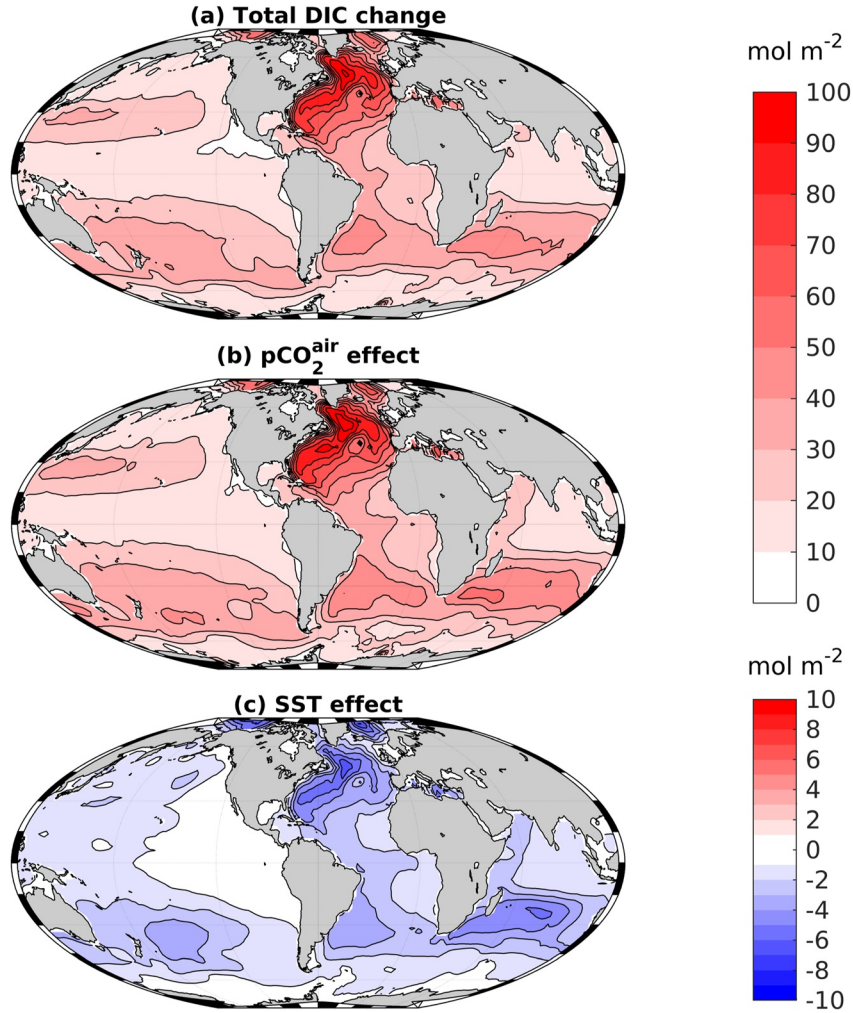

Figure 3. (a) Depth-integrated dissolved inorganic carbon (DIC) inventory change in the OCIM2-48L from 1960 to 2020 (simulations D–F). (b) Same as (a), but using OCIM2-48L simulations A–C, which isolates the effect of rising atmospheric pCO_2 (along with a small contribution from changing gas transfer velocities). (c) The difference between (a) and (b), which isolates the DIC change due to a reduction in solubility driven by warming sea surface temperatures. Positive values indicate an accumulation of DIC in the ocean, and negative values indicate a loss of DIC from the ocean.

For each product, the variability about the linear trend was computed as

$$F^{\text{var}}_{CO_2}(\text{product})(t) = F_{CO_2}(\text{product})(t) - F^{trend}_{CO_2}(\text{product})(t), \quad (3)$$

where $F_{CO_2}(\text{product})(t)$ is the globally integrated air-sea CO_2 flux at year t from a particular product (one of the OCIM2-48L simulations, GOBMs, or pCO_2 interpolation products) and $F^{trend}_{CO_2}(t)$ is the linear trend fit to the globally integrated air-sea CO_2 flux for the years 1990–2020. For the OCIM2-48L simulations D–F, this variability reflects the variability driven by observed changes in atmospheric pCO_2, SST, and gas transfer velocity (Table 1). For the GOBMs and the pCO_2 interpolation products, this variability additionally comes from changes in ocean circulation and biology, and in the case of the pCO_2 interpolation products could also include variability in the outgassing of terrestrially derived carbon (Table 1).

Interannual variability of the global air-sea CO_2 flux, as measured by its temporal standard deviation, is significantly smaller in the OCIM2-48L (~0.10 PgC yr^{-1}) than the GOBMs (~0.15 PgC yr^{-1}) and pCO_2 interpolation products (~0.22 PgC yr^{-1}; Figure 4b; Table 2). The OCIM2-48L not only has a smaller magnitude of interannual variability, but also has a different temporal pattern of variability than the GOBMs and pCO_2 products

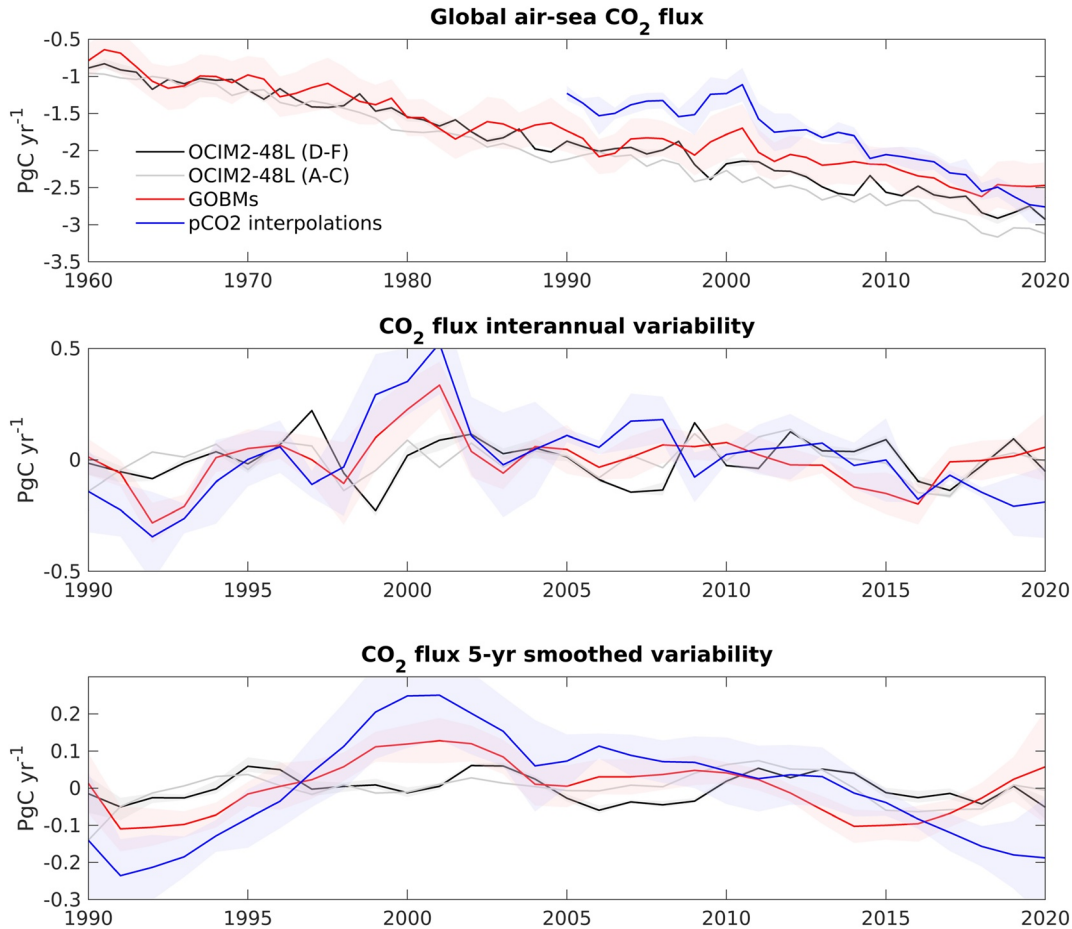

Figure 4. (a) Air-sea CO_2 fluxes for the period 1960–2020 from the OCIM2-48L (simulations D–F in black; simulations A–C in gray), global ocean biogeochemical models (GOBMs), and pCO_2 interpolation flux products. Line is the annual mean, and shading is one standard deviation (for GOBMs and pCO_2 interpolations) or the ensemble range (for OCIM2-48L). (b) Interannual variability of the global air-sea CO_2 fluxes from 1990 to 2020 computed from the various methods using Equation 3. Line is the annual mean with shading representing the uncertainty as in panel (a). (c) Variability from panel (b) after applying a 5-year moving average. Line is the mean with shading representing the uncertainty.

(Figure 4b). The interannual variability of air-sea CO_2 fluxes in the OCIM2-48L is uncorrelated with that in the GOBMs ($r = 0.14 \pm 0.18$) and the pCO_2 interpolation products ($r = -0.02 \pm 0.04$). The lack of correlation between the air-sea CO_2 fluxes in the OCIM2-48L and those in the GOBMs and pCO_2 interpolation products at the interannual timescale is predominantly due to an anticorrelation of the SST-driven and DIC-driven air-sea CO_2 fluxes in the ETP, the region that dominates global interannual variability of the ocean CO_2 sink (Rödenbeck et al., 2015). In this region, interannual variability is dominated by the El Nino Southern Oscillation (ENSO). During El Nino periods, weak upwelling leads to warmer SST, which increases the efflux of natural CO_2; at the

Table 2
Mean, Trend, and Variability of the Global Air-Sea CO_2 Flux From 1990 to 2020

	Mean	Trend	Interannual variability	5-year variability
Model	(PgC yr^{-1})	(PgC yr^{-2})	(PgC yr^{-1})	(PgC yr^{-1})
OCIM2-48L (D–F)	-2.37 ± 0.02	-0.034 ± 0.001	0.101 ± 0.002	0.039 ± 0.003
GOBMs	-2.1 ± 0.3	-0.026 ± 0.002	0.15 ± 0.03	0.09 ± 0.02
pCO_2 interpolations	-1.83 ± 0.05	-0.050 ± 0.008	0.22 ± 0.05	0.16 ± 0.05

same time, however, weaker upwelling leads to a decrease in surface DIC concentrations, which reduces the efflux of natural CO_2 (Takahashi et al., 2002). During the La Nina phase, the situation is reversed. The OCIM2-48L only captures the SST-driven component of the natural air-sea CO_2 flux variations and is therefore anticorrelated with the other products in this region.

The influence of short-term climate modes, such as ENSO, can be filtered out by taking the 5-year running mean of the global air-sea CO_2 flux variability (Figure 4c). The dominant feature in the 5-year smoothed variability of the pCO_2 interpolation products is a weakening trend in the ocean CO_2 sink during the 1990s and a strengthening trend after 2000. This feature is also present in the GOBM reconstructions although it is less pronounced (Figure 4c; DeVries et al., 2019). However, this feature does not occur in the OCIM2-48L reconstructions, neither those that include SST variability nor those that do not (Figure 4c). In general, like the interannual variability, the 5-year smoothed variability in the OCIM2-48L is much smaller than and uncorrelated with the variability in the GOBMs and pCO_2 interpolation products. The 5-year smoothed variability is roughly 0.04 PgC yr^{-1} in the OCIM2-48L simulations with pCO_2 and SST variability, roughly half the variability of the GOBMs (0.09 PgC yr^{-1}) and fourfold less than the variability of the GOBMs (0.16 PgC yr^{-1}). Furthermore, the correlation between the 5-year smoothed variability of the OCIM and GOBMs is $r = 0.15 \pm 0.19$ and between the OCIM and the pCO_2 products is $r = 0.25 \pm 0.08$.

The results in Figure 4 make it clear that the decadal variability of the ocean CO_2 sink, including the weakening trend during the 1990s and strengthening trend after 2000, is not due to the variability of atmospheric pCO_2 and SST alone. This conclusion contrasts with that of McKinley et al. (2020), who found that a single-box ocean model with a constant circulation was able to recreate the observed decadal variability of the ocean CO_2 sink when forced with the observed atmospheric pCO_2 and a globally constant temperature perturbation based on the forced SST response to volcanoes in the CESM large ensemble (Eddebbar et al., 2019). All models, including the OCIM, GOBMs, and the single-box model, have similar responses to atmospheric CO_2 forcing (McKinley et al., 2020). The main influence of atmospheric CO_2 on the 5-year smoothed variability is a weakening CO_2 sink in the early 1990s (Figure 4c), an effect also identified by McKinley et al. (2020) in the single-box model and also present in the OCIM1 (Figure S5 in Supporting Information S1). However, this effect cannot produce the whole-decade weakening of the ocean CO_2 sink during the 1990s, nor the strengthening trend thereafter (Figure 4c).

The main difference then between the OCIM2-48L and box model results of McKinley et al. (2020) can be tied to the response to the different SSTs used in each model. An important consideration is whether these models can reproduce observed subsurface ocean heat content (OHC) anomalies before and after the Pinatubo eruption as these anomalies will be tied to the air-sea heat fluxes that drive variability in both the SST and the air-sea CO_2 flux (Eddebbar et al., 2019). In the OCIM2-48L with observed SSTs, the upper-ocean (0–300 m) OHC drops by 5–10 ZJ roughly three years after the Pinatubo eruption, which is within the range but on the lower end of the cooling in observation-based reconstructions, which show a drop of between 6 and 22 ZJ over this time (Bagnell & DeVries, 2021; Cheng et al., 2017; Ishii et al., 2017; Levitus et al., 2012; Figure S7 in Supporting Information S1). In both the OCIM2-48L and the observation-based reconstructions, the negative OHC anomaly recovers to near zero by about 1996. In contrast, the single-box model of McKinley et al. (2020), when using an idealized SST perturbation derived from the volcano-forced response of the CESM large ensemble, predicts a much larger negative OHC anomaly of 55 ZJ three years after the Pinatubo eruption, and this anomaly is still roughly −30 ZJ at 1996 and persists beyond year 2000 (Figure S7 in Supporting Information S1). These results show that the OCIM2-48L adequately captures the observed subsurface heat content anomalies due to the Pinatubo eruption, while the box model with volcano-forced SST response shows a larger magnitude and greater duration of cooling than observed. However, the OCIM2-48L simulations do show a much larger increase than that observed in upper-ocean OHC around 1997–1998, coinciding with a strong El Nino event (Figure S7 in Supporting Information S1). This discrepancy likely results from ocean circulation changes that resulted in large amounts of heat being released from the upper 300 m of the Pacific Ocean to the atmosphere (Chen & Tung, 2014). These circulation changes are not captured by the steady-state OCIM2-48L.

4. Conclusions and Future Directions

This study quantified abiotic air-sea CO_2 fluxes using an ocean circulation inverse model (OCIM2-48L), accounting for the effects of changing atmospheric CO_2 concentrations, SST, and gas transfer velocity on air-sea CO_2 fluxes. The results demonstrate that the ocean absorbed CO_2 at a rate of $\sim 2.2 \pm 0.1$ PgC yr^{-1} over the period 1994–2007 with an increase in the global oceanic DIC inventory of 117 ± 4 PgC from 1960 to 2020. Over the most recent three decades (1990–2020), decadal variability of air-sea CO_2 fluxes in the OCIM has been significantly less than and poorly correlated with fluxes diagnosed from GOBMs and pCO_2-based interpolation products. These results suggest that processes that were not included in the OCIM2-48L simulations, such as changes in ocean circulation or the biological carbon pump, are more important than changes in atmospheric pCO_2 or SST in driving recent decadal variability of the ocean CO_2 sink.

These conclusions rely on the assumption that the models and data-based products used here accurately reflect the true variability of the ocean CO_2 sink as driven by the mechanisms captured by each model. Nevertheless, each approach is subject to uncertainties and structural biases that should be kept in mind when interpreting the results. For the OCIM2-48L, the main weakness is a lack of seasonality in the circulation component of the model, particularly with respect to seasonal variability in surface mixed layer depths, which could bias the results. For the biogeochemical models, structural biases are potentially introduced by inaccurate forcing fields, by parameterizations of biological processes and physical circulation processes (Hauck et al., 2015), and by model spin-up procedures (Séférian et al., 2016). For the pCO_2 interpolation products, artifacts can be introduced by the interpolation of sparse pCO_2 data (Gloege et al., 2021; Gregor et al., 2019; Rödenbeck et al., 2015), and additional uncertainty is introduced by the input products and formulations used for the bulk air-sea gas exchange formula (Fay et al., 2021; Roobaert et al., 2018; Watson et al., 2020). Using an ensemble of different products, as done here, reduces the influence of these sources of error if they are randomly distributed, but any common biases across products within each method could bias the conclusions presented here. Therefore, future work should put a priority on identifying and ameliorating any sources of structural bias in these different methods.

One aspect that is not addressed in this analysis is whether circulation or biological processes, such as primary production and particle export, are more important for driving variability of the air-sea CO_2 flux. Future work should put a high priority on building models that can capture the observed variability in both circulation and biology in order to determine how these factors have responded to recent climate change and natural climate variability. Likewise, the variability of carbon fluxes at boundaries other than the air-sea interface should be investigated as this impacts the air-sea CO_2 fluxes inferred from seawater pCO_2 observations. Developing additional independent methods for quantifying air-sea CO_2 fluxes from observations, such as data-based models that capture observed changes in ocean internal DIC and alkalinity distributions, should also be a target of future work.

Data Availability Statement

Data from the 2021 Global Carbon Budget used in this study are available from the Global Carbon Project at https://doi.org/10.18160/gcp-2021 (Global Carbon Project, 2021). Atmospheric CO_2 time series data used in this study are available from National Atmospheric and Oceanic Administration (NOAA) stations at the South Pole (https://gml.noaa.gov/aftp/data/trace_gases/co2/flask/surface/co2_spo_surface-flask_1_ccgg_month.txt), American Samoa (https://gml.noaa.gov/aftp/data/trace_gases/co2/flask/surface/co2_smo_surface-flask_1_ccgg_month.txt), Mauna Loa (https://gml.noaa.gov/webdata/ccgg/trends/co2/co2_mm_mlo.txt), and Barrow, Alaska (https://gml.noaa.gov/aftp/data/trace_gases/co2/flask/surface/co2_brw_surface-flask_1_ccgg_month.txt), and from the Law Dome ice core (https://scrippsco2.ucsd.edu/assets/data/atmospheric/merged_ice_core_mlo_spo/merged_ice_core_yearly.csv). Wind speed, sea ice, and sea level pressure data used in this study are available from the National Centers for Environmental Prediction (NCEP) monthly reanalysis at https://psl.noaa.gov/thredds/catalog/Datasets/ncep.reanalysis/surface_gauss/catalog.html. Sea surface temperature (SST) reconstructions used in this study are available from the Hadley Centre (https://www.metoffice.gov.uk/hadobs/hadisst/index.html), the Japan Meteorological Agency (JMA; https://psl.noaa.gov/data/gridded/data.cobe.html), and NOAA (https://psl.noaa.gov/data/gridded/data.noaa.ersst.v5.html). Subsurface ocean temperature anomaly data used in this study are available from NOAA (https://www.ncei.noaa.gov/access/global-ocean-heat-content/anomaly_data_t.html), the Institute of Atmospheric Physics (IAP; ftp://www.ocean.iap.ac.cn/cheng/CZ16_v3_IAP_

Temperature_anomaly_gridded_1month_netcdf/) which can also be accessed at http://www.ocean.iap.ac.cn/pages/dataService/dataService.html?navAnchor=dataService), JMA (https://climate.mri-jma.go.jp/pub/ocean/ts/v7.3.1/temp/grib2/), and the Autoregressive Artificial Neural Network (ARANN; https://doi.org/10.6084/m9.figshare.12959489.v6). The OCIM2-48L model output is publicly available on the FigShare database under accession code doi.org/10.6084/m9.figshare.19341974.

Acknowledgments
The author thanks Nicolas Gruber and Galen McKinley for constructive reviews that improved the manuscript. The author acknowledges support from NSF grant OCE-1948955.

References

Aumont, O., Éthé, C., Tagliabue, A., Bopp, L., & Gehlen, M. (2015). PISCES-v2: An ocean biogeochemical model for carbon and ecosystem studies. *Geoscientific Model Development Discussions*, *8*(2). https://doi.org/10.5194/gmd-8-2465-2015

Bagnell, A., & DeVries, T. (2021). 20th century cooling of the deep ocean contributed to delayed acceleration of Earth's energy imbalance. *Nature Communications*, *12*(1), 1–10. https://doi.org/10.1038/s41467-021-24472-3

Bakker, D. C. E., Pfeil, B., Landa, C. S., Metzl, N., O'Brien, K. M., Olsen, A., & Xu, S. (2016). A multi-decade record of high-quality fCO_2 data in version 3 of the Surface Ocean CO_2 Atlas (SOCAT). *Earth System Science Data*, *8*, 383–413.

Behringer, D., & Xue, Y. (2004). Evaluation of the global ocean data assimilation system at NCEP: The Pacific Ocean. In *Proc. eighth symp. on integrated observing and assimilation systems for atmosphere, oceans, and land surface*.

Berthet, S., Séférian, R., Bricaud, C., Chevallier, M., Voldoire, A., & Ethé, C. (2019). Evaluation of an online grid-coarsening algorithm in a global eddy-admitting ocean biogeochemical model. *Journal of Advances in Modeling Earth Systems*, *11*(6), 1759–1783. https://doi.org/10.1029/2019ms001644

Chafik, L., Hátún, H., Kjellsson, J., Larsen, K. M. H., Rossby, T., & Berx, B. (2020). Discovery of an unrecognized pathway carrying overflow waters toward the Faroe Bank Channel. *Nature Communications*, *11*(1), 1–10. https://doi.org/10.1038/s41467-020-17426-8

Chau, T. T. T., Gehlen, M., & Chevallier, F. (2021). A seamless ensemble-based reconstruction of surface ocean pCO_2 and air–sea CO_2 fluxes over the global coastal and open oceans. *Biogeosciences Discussions*, 1–30.

Chen, X., & Tung, K.-K. (2014). Varying planetary heat sink led to global-warming slowdown and acceleration. *Science*, *345*(6199), 897–903. https://doi.org/10.1126/science.1254937

Cheng, L., Trenberth, K. E., Fasullo, J., Boyer, T., Abraham, J., & Zhu, J. (2017). Improved estimates of ocean heat content from 1960 to 2015. *Science Advances*, *3*(3), e1601545. https://doi.org/10.1126/sciadv.1601545

de Lavergne, C., Falahat, S., Madec, G., Roquet, F., Nycander, J., & Vic, C. (2019). Toward global maps of internal tide energy sinks. *Ocean Modelling*, *137*, 52–75. https://doi.org/10.1016/j.ocemod.2019.03.010

de Lavergne, C., Vic, C., Madec, G., Roquet, F., Waterhouse, A. F., Whalen, C., & Hibiya, T. (2020). A parameterization of local and remote tidal mixing. *Journal of Advances in Modeling Earth Systems*, *12*(5), e2020MS002065. https://doi.org/10.1029/2020ms002065

DeVries, T. (2014). The oceanic anthropogenic CO_2 sink: Storage, air-sea fluxes, and transports over the industrial era. *Global Biogechem. Cycles*, *28*, 631–647. https://doi.org/10.1002/2013gb004739

DeVries, T., & Holzer, M. (2019). Radiocarbon and helium isotope constraints on deep ocean ventilation and mantle-3He sources. *Journal of Geophysical Research: Oceans*, *124*(5), 3036–3057. https://doi.org/10.1029/2018jc014716

DeVries, T., Holzer, M., & Primeau, F. (2017). Recent increase in oceanic carbon uptake driven by weaker upper-ocean overturning. *Nature*, *542*(7640), 215–218. https://doi.org/10.1038/nature21068

DeVries, T., Le Quéré, C., Andrews, O., Berthet, S., Hauck, J., Ilyina, T., et al. (2019). Decadal trends in the ocean carbon sink. *Proceedings of the National Academy of Sciences*, *116*(24), 11646–11651. https://doi.org/10.1073/pnas.1900371116

DeVries, T., & Primeau, F. (2011). Dynamically and observationally constrained estimates of water-mass distributions and ages in the global ocean. *Journal of Physical Oceanography*, *41*, 2381–2401. https://doi.org/10.1175/JPO-D-10-05011.1

DeVries, T., & Weber, T. (2017). The export and fate of organic matter in the ocean: New constraints from combining satellite and oceanographic tracer observations. *Global Biogeochemical Cycles*, *31*(3), 535–555. https://doi.org/10.1002/2016gb005551

Doney, S. C., Lima, I., Feely, R. A., Glover, D. M., Lindsay, K., Mahowald, N., et al. (2009). Mechanisms governing interannual variability in upper-ocean inorganic carbon system and air–sea CO_2 fluxes: Physical climate and atmospheric dust. *Deep Sea Research Part II: Topical Studies in Oceanography*, *56*(8–10), 640–655. https://doi.org/10.1016/j.dsr2.2008.12.006

Eddebbar, Y. A., Rodgers, K. B., Long, M. C., Subramanian, A. C., Xie, S.-P., & Keeling, R. F. (2019). El Niño–like physical and biogeochemical ocean response to tropical eruptions. *Journal of Climate*, *32*(9), 2627–2649. https://doi.org/10.1175/jcli-d-18-0458.1

Fay, A. R., Gregor, L., Landschützer, P., McKinley, G. A., Gruber, N., Gehlen, M., & Zeng, J. (2021). Harmonization of global surface ocean pco_2 mapped products and their flux calculations; an improved estimate of the ocean carbon sink. *Earth System Science Data Discussions*, 1–32.

Friedlingstein, P., Jones, M. W., O'Sullivan, M., Andrew, R. M., Bakker, D. C. E., Hauck, J., et al. (2021). Global carbon budget 2021. *Earth System Science Data Discussions*, *2021*, 1–191. https://doi.org/10.5194/essd-2021-386

Friedlingstein, P., Jones, M. W., O'Sullivan, M., Andrew, R. M., Hauck, J., Peters, G. P., & Zaehle, S. (2019). Global carbon budget 2019. *Earth System Science Data*, *11*(4), 1783–1838. https://doi.org/10.5194/essd-11-1783-2019

Fröb, F., Olsen, A., Våge, K., Moore, G., Yashayaev, I., Jeansson, E., & Rajasakaren, B. (2016). Irminger Sea deep convection injects oxygen and anthropogenic carbon to the ocean interior. *Nature Communications*, *7*(1), 1–8. https://doi.org/10.1038/ncomms13244

Global Carbon Project. (2021). Supplemental data of global carbon budget 2021 (Version 1.0) [Data set]. *Global Carbon Project*.

Gloege, L., McKinley, G. A., Landschützer, P., Fay, A. R., Frölicher, T. L., Fyfe, J. C., & Schlunneger, S. (2021). Quantifying errors in observationally based estimates of ocean carbon sink variability. *Global Biogeochemical Cycles*, *35*(4), e2020GB006788. https://doi.org/10.1029/2020gb006788

Gregor, L., Lebehot, A. D., Kok, S., & Monteiro, P. M. S. (2019). A comparative assessment of the uncertainties of global surface ocean CO_2 estimates using a machine-learning ensemble (CSIR-ML6 version 2019a)—Have we hit the wall? *Geoscientific Model Development*, *12*(12), 5113. https://doi.org/10.5194/gmd-12-5113-2019

Gruber, N., Clement, D., Carter, B. R., Feely, R. A., vanHeuven, S., Hoppema, M., et al. (2019). The oceanic sink for anthropogenic CO_2 from 1994 to 2007. *Science*, *363*(6432), 1193–1199. https://doi.org/10.1126/science.aau5153

Gruber, N., Landschützer, P., & Lovenduski, N. S. (2019). The variable Southern Ocean carbon sink. *Annual Review of Marine Science*, *11*, 159–186. https://doi.org/10.1146/annurev-marine-121916-063407

Hauck, J., Völker, C., Wolf-Gladrow, D. A., Laufkötter, C., Vogt, M., Aumont, O., et al. (2015). On the Southern Ocean CO_2 uptake and the role of the biological carbon pump in the 21st century. *Global Biogeochemical Cycles*, *29*(9), 1451–1470. https://doi.org/10.1002/2015gb005140

Hauck, J., Zeising, M., Le Quéré, C., Gruber, N., Bakker, D. C., Bopp, L., et al. (2020). Consistency and challenges in the ocean carbon sink estimate for the global carbon budget. *Frontiers in Marine Science*, 852. https://doi.org/10.3389/fmars.2020.571720

Holzer, M., DeVries, T., & de Lavergne, C. (2021). Diffusion controls the ventilation of a Pacific shadow zone above abyssal overturning. *Nature Communications*, *12*(1), 1–13. https://doi.org/10.1038/s41467-021-24648-x

Ishii, M., Fukuda, Y., Hirahara, S., Yasui, S., Suzuki, T., & Sato, K. (2017). Accuracy of global upper ocean heat content estimation expected from present observational data sets. *Solanus*, *13*, 163–167. https://doi.org/10.2151/sola.2017-030

Khatiwala, S., Primeau, F., & Hall, T. (2009). Reconstruction of the history of anthropogenic CO_2 concentrations in the ocean. *Nature*, *462*(7271), 346–349. https://doi.org/10.1038/nature08526

Khatiwala, S., Tanhua, T., Mikaloff Fletcher, S., Gerber, M., Doney, S. C., Graven, H. D., et al. (2013). Global ocean storage of anthropogenic carbon. *Biogeosciences*, *10*(4), 2169–2191. https://doi.org/10.5194/bg-10-2169-2013

Khatiwala, S., Visbeck, M., & Cane, M. A. (2005). Accelerated simulation of passive tracers in ocean circulation models. *Ocean Modelling*, *9*(1), 51–69. https://doi.org/10.1016/j.ocemod.2004.04.002

Kwon, E. Y., DeVries, T., Galbraith, E. D., Hwang, J., Kim, G., & Timmermann, A. (2021). Stable carbon isotopes suggest large terrestrial carbon inputs to the global ocean. *Global Biogeochemical Cycles*, *35*(4), e2020GB006684. https://doi.org/10.1029/2020gb006684

Kwon, E. Y., & Primeau, F. (2006). Optimization and sensitivity study of a biogeochemistry ocean model using an implicit solver and in situ phosphate data. *Global Biogeochemical Cycles*, *20*(4). https://doi.org/10.1029/2005gb002631

Lacroix, F., Ilyina, T., Mathis, M., Laruelle, G. G., & Regnier, P. (2021). Historical increases in land-derived nutrient inputs may alleviate effects of a changing physical climate on the oceanic carbon cycle. *Global Change Biology*, *27*(21), 5491–5513. https://doi.org/10.1111/gcb.15822

Landschützer, P., Gruber, N., & Bakker, D. C. (2016). Decadal variations and trends of the global ocean carbon sink. *Global Biogeochemical Cycles*, *30*(10), 1396–1417. https://doi.org/10.1002/2015gb005359

Landschützer, P., Gruber, N., Haumann, F. A., Rödenbeck, C., Bakker, D. C. E., van Heuven, S., et al. (2015). The reinvigoration of the Southern Ocean carbon sink. *Science*, *349*(6253), 1221–1224. https://doi.org/10.1126/science.aab2620

Lauvset, S. K., Key, R. M., Olsen, A., van Heuven, S., Velo, A., Lin, X., & Watelet, S. (2016). A new global interior ocean mapped climatology: The 1 × 1 GLODAP version 2. *Earth System Science Data*, *8*(2), 325–340. https://doi.org/10.5194/essd-8-325-2016

Levitus, S., Antonov, J. I., Boyer, T. P., Baranova, O. K., Garcia, H. E., Locarnini, R. A., et al. (2012). World ocean heat content and thermosteric sea level change (0–2000 m), 1955–2010. *Geophysical Research Letters*, *39*(10). https://doi.org/10.1029/2012gl051106

Liao, E., Resplandy, L., Liu, J., & Bowman, K. W. (2020). Amplification of the ocean carbon sink during El Niños: Role of poleward ekman transport and influence on atmospheric CO_2. *Global Biogeochemical Cycles*, *34*(9), e2020GB006574. https://doi.org/10.1029/2020gb006574

Macfarling Meure, C., Etheridge, D., Trudinger, C., Steele, P., Langenfelds, R., Van Ommen, T., et al. (2006). Law Dome CO_2, CH_4 and N_2O ice core records extended to 2000 years BP. *Geophysical Research Letters*, *33*(14). https://doi.org/10.1029/2006gl026152

McKinley, G. A., Fay, A. R., Eddebbar, Y. A., Gloege, L., & Lovenduski, N. S. (2020). External forcing explains recent decadal variability of the ocean carbon sink. *AGU Advances*, *1*(2), e2019AV000149. https://doi.org/10.1029/2019av000149

Mikaloff Fletcher, S. E., Gruber, N., Jacobson, A. R., Doney, S. C., Dutkiewicz, S., Gerber, M., et al. (2006). Inverse estimates of anthropogenic CO_2 uptake, transport, and storage by the ocean. *Global Biogeochemical Cycles*, *20*(2). https://doi.org/10.1029/2005gb002530

Murata, A., Kumamoto, Y., Sasaki, K.-i., Watanabe, S., & Fukasawa, M. (2009). Decadal increases of anthropogenic CO_2 along 149°E in the Western North Pacific. *Journal of Geophysical Research*, *114*(C4). https://doi.org/10.1029/2008jc004920

Resplandy, L., Keeling, R., Rödenbeck, C., Stephens, B., Khatiwala, S., Rodgers, K., et al. (2018). Revision of global carbon fluxes based on a reassessment of oceanic and riverine carbon transport. *Nature Geoscience*, *11*(7), 504–509. https://doi.org/10.1038/s41561-018-0151-3

Rhein, M., Fischer, J., Smethie, W. M., Smythe-Wright, D., Weiss, R. F., Mertens, C., et al. (2002). Labrador sea water: Pathways, cfc inventory, and formation rates. *Journal of Physical Oceanography*, *32*(2), 648–665. https://doi.org/10.1175/1520-0485(2002)032<0648:lswpci>2.0.co;2

Rödenbeck, C., Bakker, D. C., Metzl, N., Olsen, A., Sabine, C., Cassar, N., & Heimann, M. (2014). Interannual sea–air CO_2 flux variability from an observation-driven ocean mixed-layer scheme. *Biogeosciences*, *11*, 4599–4613. https://doi.org/10.5194/bg-11-4599-2014

Rödenbeck, C., Bakker, D. C. E., Gruber, N., Iida, Y., Jacobson, A. R., Jones, S., & Zeng, J. (2015). Data-based estimates of the ocean carbon sink variability–first results of the Surface Ocean pCO_2 Mapping intercomparison (SOCOM). *Biogeosciences*, *12*, 7251–7278. https://doi.org/10.5194/bg-12-7251-2015

Roobaert, A., Laruelle, G. G., Landschützer, P., & Regnier, P. (2018). Uncertainty in the global oceanic CO_2 uptake induced by wind forcing: Quantification and spatial analysis. *Biogeosciences*, *15*(6), 1701–1720. https://doi.org/10.5194/bg-15-1701-2018

Sabine, C. L., Feely, R. A., Gruber, N., Key, R. M., Lee, K., Bullister, J. L., et al. (2004). The oceanic sink for anthropogenic CO_2. *Science*, *305*(5682), 367–371. https://doi.org/10.1126/science.1097403

Sarmiento, J. L., Orr, J. C., & Siegenthaler, U. (1992). A perturbation simulation of CO_2 uptake in an ocean general circulation model. *Journal of Geophysical Research*, *97*(C3), 3621–3645. https://doi.org/10.1029/91jc02849

Schlitzer, R. (1993). Determining the mean, large-scale circulation of the Atlantic with the adjoint method. *Journal of Physical Oceanography*, *23*(9), 1935–1952. https://doi.org/10.1175/1520-0485(1993)023<1935:dtmlsc>2.0.co;2

Schlitzer, R. (2007). Assimilation of radiocarbon and chlorofluorocarbon data to constrain deep and bottom water transports in the world ocean. *Journal of Physical Oceanography*, *37*(2), 259–276. https://doi.org/10.1175/jpo3011.1

Schwinger, J., Goris, N., Tjiputra, J. F., Kriest, I., Bentsen, M., Bethke, I., et al. (2016). Evaluation of NorESM-OC (versions 1 and 1.2), the ocean carbon-cycle stand-alone configuration of the Norwegian Earth System Model (NorESM1). *Geoscientific Model Development*, *9*, 2589–2622. https://doi.org/10.5194/gmd-9-2589-2016

Séférian, R., Gehlen, M., Bopp, L., Resplandy, L., Orr, J. C., Marti, O., et al. (2016). Inconsistent strategies to spin up models in CMIP5: Implications for ocean biogeochemical model performance assessment. *Geoscientific Model Development*, *9*(5), 1827–1851. https://doi.org/10.5194/gmd-9-1827-2016

Takahashi, T., Sutherland, S. C., Sweeney, C., Poisson, A., Metzl, N., Tilbrook, B., & Nojiri, Y. (2002). Global sea–air CO_2 flux based on climatological surface ocean pCO_2, and seasonal biological and temperature effects. *Deep Sea Research Part II: Topical Studies in Oceanography*, *49*(9), 1601–1622. (The Southern Ocean I: Climatic Changes in the Cycle of Carbon in the Southern Ocean). https://doi.org/10.1016/S0967-0645(02)00003-6

Wanninkhof, R., Park, G.-H., Takahashi, T., Sweeney, C., Feely, R., Nojiri, Y., et al. (2013). Global Ocean carbon uptake: Magnitude, variability and trends. *Biogeosciences*, *10*(3), 1983–2000. https://doi.org/10.5194/bg-10-1983-2013

Waters, J. F., Millero, F. J., & Sabine, C. L. (2011). Changes in South Pacific anthropogenic carbon. *Global Biogeochemical Cycles*, *25*(4). https://doi.org/10.1029/2010gb003988

Watson, A. J., & Orr, J. C. (2003). Carbon dioxide fluxes in the global ocean. In *Ocean biogeochemistry* (pp. 123–143). Springer. https://doi.org/10.1007/978-3-642-55844-3_6

Watson, A. J., Schuster, U., Shutler, J. D., Holding, T., Ashton, I. G., Landschützer, P., et al. (2020). Revised estimates of ocean-atmosphere CO_2 flux are consistent with ocean carbon inventory. *Nature Communications*, *11*(1), 1–6. https://doi.org/10.1038/s41467-020-18203-3

Wright, R. M., Le Quéré, C., Buitenhuis, E., Pitois, S., & Gibbons, M. J. (2021). Role of jellyfish in the plankton ecosystem revealed using a global ocean biogeochemical model. *Biogeosciences*, *18*(4), 1291–1320. https://doi.org/10.5194/bg-18-1291-2021

Zweng, M., Reagan, J., Antonov, J., Locarnini, R., Mishonov, A., Boyer, T., et al. (2013). World Ocean Atlas 2013, volume 2: Salinity. In S. Levitus, & A. Mishonov (Eds.), *NOAA Atlas NESDIS* (Vol. 74).

References From the Supporting Information

Dlugokencky, E., Mund, J., Crotwell, A., Crotwell, M., & Thoning, K. (2020). *Atmospheric carbon dioxide dry air mole fractions from the NOAA GML carbon cycle cooperative global air sampling networkversion: 2020-07 (Tech. Rep.)*. https://doi.org/10.15138/wkgj-f215

Graven, H., Gruber, N., Key, R., Khatiwala, S., & Giraud, X. (2012). Changing controls on oceanic radiocarbon: New insights on shallow-to-deep ocean exchange and anthropogenic CO_2 uptake. *Journal of Geophysical Research*, *117*(C10).

Guilderson, T., Schrag, D., Fallon, S., Dunbar, R., Kilbourne, K., & Prouty, N. G. (2005). *Surface Water Radiocarbon (Delta14C) Reconstructed from Reef-Building Zooxanthellate Corals from 1751-2004 (Tech. Rep.). Oak Ridge, Tennessee*. Retrieved from http://cdiac.ornl.gov/ftp/oceans/coralC14_data/

Huang, B., Banzon, V. F., Freeman, E., Lawrimore, J., Liu, W., Peterson, T. C., & Zhang, H.-M. (2015). Extended reconstructed sea surface temperature version 4 (ERSST. v4). Part I: Upgrades and intercomparisons. *Journal of climate*, *28*(3), 911–930.

Ishii, M., Shouji, A., Sugimoto, S., & Matsumoto, T. (2005). Objective analyses of sea-surface temperature and marine meteorological variables for the 20th century using ICOADS and the Kobe collection. *International Journal of Climatology: A Journal of the Royal Meteorological Society*, *25*(7), 865–879.

Kalnay, E., Kanamitsu, M., Kistler, R., Collins, W., Deaven, D., Gandin, L., & Joseph, D. (1996). The NCEP/NCAR 40-year reanalysis project. *Bulletin of the American meteorological Society*, *77*(3), 437–472.

Large, W. G., McWilliams, J. C., & Doney, S. C. (1994). Oceanic vertical mixing: A review and a model with a nonlocal boundary layer parameterization. *Reviews of Geophysics*, *32*(4), 363–403.

Lewis, E., & Wallace, D. (1998). Program developed for CO_2 system calculations. Oak Ridge National Laboratory.

Li, X., & Primeau, F. W. (2008). A fast Newton–Krylov solver for seasonally varying global ocean biogeochemistry models. *Ocean Modelling*, *23*(1-2), 13–20.

Locarnini, R., Mishonov, A., Antonov, J., Boyer, T., Garcia, H., Baranova, O., & Seidov, D. (2013). World Ocean Atlas 2013, Volume 1: Temperature. In S. Levitus, & A. Mishonov (Eds.), *NOAA Atlas NESDIS* (Vol. 73).

Olsen, A., Key, R. M., van Heuven, S., Lauvset, S. K., Velo, A., Lin, X., & Suzuki, T. (2016). The Global Ocean Data Analysis Project version 2 (GLODAPv2) – an internally consistent data product for the world ocean. *Earth System Science Data*, *8*(2), 297–323. https://doi.org/10.5194/essd-8-297-2016

Rayner, N., Parker, D. E., Horton, E., Folland, C. K., Alexander, L. V., Rowell, D., & Kaplan, A. (2003). Global analyses of sea surface temperature, sea ice, and night marine air temperature since the late nineteenth century. *Journal of Geophysical Research*, *108*(D14).